An MPC-based attitude control system for all-electric spacecraft with on/off actuators

Mirko Leomanni¹, Andrea Garulli¹, Antonio Giannitrapani¹, Fabrizio Scortecci²

Abstract—Pointing accuracy is a key requirement in communication satellites and Earth observation missions. Attitude control systems must guarantee tracking of the reference attitude and angular rate, while accounting for mission performance indexes such as fuel consumption and actuator wear. In this paper, an MPC-based attitude control scheme is proposed for an all-electric spacecraft using cold gas and resistojet thrusters as on/off actuators for attitude control. This technology imposes restrictions on the number of thruster firings, which are explicitly taken into account in the MPC formulation and suitably traded-off with fuel consumption. The performance of the proposed attitude control system is demonstrated on a GEO mission and compared with other control schemes involving on/off actuators.

I. Introduction

High efficiency electric propulsion (EP) systems for spacecraft orbit raising and station-keeping operations are one of the most promising technologies to provide a substantial decrease of the mission costs with respect to conventional platforms [1], [2]. While the use of EP thrusters is already well understood for precise orbit control (see, e.g., [3], [4], [5]), several alternatives are still under investigation to provide fine pointing of the spacecraft in the presence of attitude disturbances. A viable solution is represented by cold gas and resistojet thrusters which, by exploiting the same Xenon bus of the orbit maneuvering system, allow one to reduce complexity and cost of commercial platforms [6], [7]. These thrusters must be operated in on/off mode, and restrictions on the duration and number of thruster firings have to be accounted for in the design of the attitude control system (ACS). Such technological limitations typically result in oscillating behaviors of the closed-loop system [8]. Since the amplitude of these oscillations is inversely proportional to the number of thruster firings, achieving precise attitude control while retaining an acceptable number of switching cycles is a challenging task.

A wide variety of control techniques have been proposed in the literature for ACS design based on on/off actuators, including bang-bang control [9], linear quadratic regulators (LQR) with pulse-width pulse-frequency modulators (PWPF) [10], [11], [12], mixed-integer linear programming (MILP) control allocation [13], and model predictive control (MPC) [14], [15]. While many of these techniques explicitly account for switching-time constraints, they do not address

Leomanni, Garulli and Giannitrapani A. with the Dipartimento di Ingegneria dell'Informazione e Scienze Matematiche, Università di Siena, Siena, Italy. Email:

the problem of minimizing the overall number of thruster firings, which has a key impact on the lifetime of the thrusters and hence of the mission itself.

In this paper, a new approach to ACS design is presented for three-axis precision pointing of an all-electric spacecraft operating in a geostationary (GEO) mission. An MPC law, based on the solution of a MILP problem, is proposed, whose objective is to keep the spacecraft attitude and angular velocity within given bounds. The main advantage of this approach compared to traditional techniques is that the number of thruster firings, as well the overall fuel consumption, are explicitly taken into account in the control design. Simulations are reported to evaluate the performance of the proposed solution, in comparison to other techniques based on on/off actuators.

The paper is organized as follows. Section II describes the reference mission, the spacecraft layout and the main features of the attitude control problem. In Section III, the attitude dynamic model is introduced, along with a detailed analysis of the disturbance torques acting on the system. In Section IV, the MPC-based attitude control law is derived. The performance of the proposed control law is evaluated through simulation tests in Section V. In Section VI, some conclusions are drawn and future directions of research are outlined.

II. PROBLEM SETTING

A. Reference frames and notation

Three reference frames are used in this work. The first one is an Earth centered inertial (ECI) frame. The other two coordinate systems are moving frames centered at the spacecraft center of mass. The so called local-vertical/local-horizontal (LVLH) frame is oriented such that its Z axis is aligned with the nadir vector, the Y axis is normal to the orbital plane and the X axis completes an orthogonal right handed frame. The body frame, whose axes are conventionally referred to as roll, pitch and yaw axes, is aligned with the principal axes of inertia of the spacecraft. The desired attitude during the spacecraft orbital motion is such that the body and the LVLH frame overlap, as depicted in Figure 1.

Vector and matrices are denoted by boldface symbols. The symbol 0 denotes a vector whose components are all equal to 0. Similarly, 1 is a vector whose components are all equal to 1. The identity matrix of order n is denoted by I_n . The orientation of reference frame B with respect to reference frame A is expressed by the rotation matrix $\mathbf{R}_{\mathbf{A}\mathbf{B}}$ or, equivalently, by the quaternion $\mathbf{q}_{\mathbf{A}\mathbf{B}}$. The scalar

Italy. Email: fscortecci@aerospazio.com.

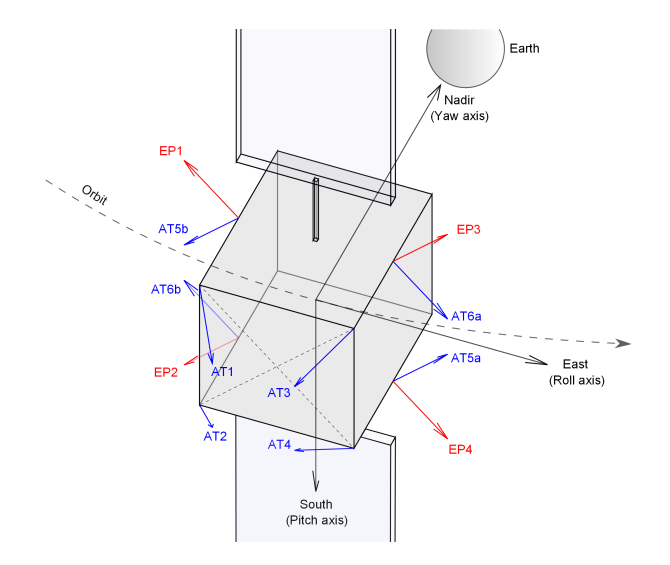


Fig. 1. Thrusters layout

portion of the quaternion is the first element and the quaternion multiplication is defined such that $\mathbf{q}_{AC} = \mathbf{q}_{BC} \circ \mathbf{q}_{AB}$ corresponds to the sequence of rotations $\mathbf{R}_{AC} = \mathbf{R}_{BC} \mathbf{R}_{AB}$. The transformation from a quaternion to a rotation matrix is denoted by $\mathbf{R}(\mathbf{q})$. Small rotations can be represented in quaternion form as $\delta \mathbf{q}(\gamma) = [1 \ , \ \gamma^T/2]^T$, where γ is a three-dimensional rotation vector.

B. Reference mission

The objective of the reference mission is to provide high accuracy attitude control of a small all-electric GEO platform in the presence of unknown disturbances. Due to a number of disturbance effects acting on the spacecraft dynamics, like the luni-solar perturbation, the Earth's aspherical gravity field and solar radiation pressure, periodic station-keeping maneuvers through EP thrusters are required. Uncertainty on the exact position of the center of mass and on the exact alignment of the thrusters causes a persistent disturbance torque which must be compensated by the ACS. The driving requirements for attitude control are:

- pointing accuracy of 1 mrad per axis;
- pointing rate accuracy of 10 μ rad/s per axis.

The first requirement is dictated by K_a band communication instruments, while the second one is typically found in Earth observation satellites carrying on-board optical payloads which are very sensitive to micro vibrations and oscillations [16].

C. Spacecraft layout

The spacecraft external layout is representative of a typical two tons small geostationary platform. The size of the main body is $2 \, \text{m} \times 2 \, \text{m} \times 2.5 \, \text{m}$ and two solar panels of dimensions $5 \, \text{m} \times 2 \, \text{m}$ are attached to the north and south faces of the bus. The considered propulsion system is illustrated in Figure 1. Four SPT-100 Hall effect thruster (HET) modules (EP1, EP2, EP3, EP4) symmetrically oriented around the nadir vector, with an angle of 45° between the north/south

axis and the thrust direction, are used for GEO orbital maneuvers. Nominally, the direction of the thrust vectors passes through the center of mass of the spacecraft. Eight on/off Xenon microthruster modules that can be operated either as cold gas thrusters (CGT) or very high temperature resistojets (VHTR) are used for real-time attitude control. Operation in VHTR mode provides an increased specific impulse I_{sp} due to heating of the exhaust gas. Four thrusters (AT1, AT2, AT3, AT4) are mounted on the anti-nadir face, with an angle of 48.5° between the diagonal of the face and the thrust direction, to maximize the lever arm and hence the torque about both the roll and pitch axes. The remaining four thruster (AT5a, AT5b, AT6a, AT6b) are symmetrically oriented around the nadir vector, with an angle of 135° between the north/south axis and the thrust direction, and fired in pairs to provide pure torques around the yaw axis. The layout of the CGT/VHTR thrusters has been deigned so as to provide an efficient rejection of the station-keeping disturbance torque generated by uncertainty on the center of mass and thruster misalignment. For any possible combination of the actual center of mass position and the EP thrust vector alignment, the pitch and roll components of the disturbance torque are coupled and have approximately the same magnitude, while the yaw component, with a larger worst-case magnitude, is almost decoupled. To avoid control torques summing up to zero, the simultaneous use of thrusters AT1-AT4, AT2-AT3 and AT5-AT6 is prevented. The basic specifications of the propulsion system are summarized in Table I.

TABLE I PROPULSION SYSTEM SPECIFICATIONS

Type	Thrust	I_{sp}	Firing Time	Power
HET	75 (mN)	1500 (s)	> 10 (min)	1350 (W)
CGT/VHTR	0.5/1.5 (mN)	30/90 (s)	> 0.5 (s)	< 20 (W)

III. ATTITUDE DYNAMIC MODEL

Let \mathbf{q}_{IB} be the quaternion representing the orientation of the spacecraft body frame with respect to the ECI frame, and $\boldsymbol{\omega}$ be the angular rate of the body frame with respect to ECI frame, expressed in the body frame. The model describing the spacecraft attitude dynamics can be written as

$$\dot{\mathbf{q}}_{IB} = \frac{1}{2} \begin{bmatrix} 0 \\ \boldsymbol{\omega} \end{bmatrix} \circ \mathbf{q}_{IB}, \tag{1}$$

$$\dot{\boldsymbol{\omega}} = \mathbf{I}_{\mathbf{M}}^{-1} \left(\boldsymbol{\tau}_d + \boldsymbol{\tau}_u - \boldsymbol{\omega} \times \mathbf{I}_{\mathbf{M}} \, \boldsymbol{\omega} - \dot{\mathbf{I}}_{\mathbf{M}} \, \boldsymbol{\omega} \right), \tag{2}$$

where \mathbf{I}_{M} is the spacecraft inertia matrix, $\boldsymbol{\tau}_d$ is the disturbance torque and $\boldsymbol{\tau}_u$ is the control torque (both expressed in the body frame). Since thrusters AT5a and AT5b, as well as thrusters AT6a and AT6b, are fired simultaneously, denoting by $\boldsymbol{\tau}_5$ and $\boldsymbol{\tau}_6$ the corresponding resulting torques, the mapping between the control torque $\boldsymbol{\tau}_u$ and the on/off activation command \mathbf{u} is given by

$$\boldsymbol{\tau}_u = \mathbf{T}\mathbf{u} = \begin{bmatrix} \boldsymbol{\tau}_1 & \boldsymbol{\tau}_2 & \boldsymbol{\tau}_3 & \boldsymbol{\tau}_4 & \boldsymbol{\tau}_5 & \boldsymbol{\tau}_6 \end{bmatrix} \mathbf{u}, \quad (3)$$

where $\mathbf{u} = [u_1, ..., u_6]^T$, with $u_i \in \{0, 1\}$. Given the thruster alignments, the matrix **T** has the following structure

$$\mathbf{T} = \bar{f} \begin{bmatrix} -d_{xy} & d_{xy} & -d_{xy} & d_{xy} & 0 & 0 \\ d_{xy} & d_{xy} & -d_{xy} & -d_{xy} & 0 & 0 \\ 0 & 0 & 0 & 0 & d_z & -d_z \end{bmatrix}, (4)$$

where \bar{f} is the nominal thrust magnitude and d_{xy} , d_z are constant lever arms. The propellant mass rate, resulting from thrusters operation, is

$$\dot{m} = -\frac{\bar{f} \parallel \mathbf{\Lambda} \mathbf{u} \parallel_1}{g I_{sp}},\tag{5}$$

where g is the gravity acceleration and the matrix $\Lambda = \text{diag}([1, 1, 1, 1, 2, 2])$ accounts for the specific thruster configuration.

A detailed analysis of the disturbance torques τ_d in (2) has been performed, taking into account gravity gradient, solar radiation pressure and station-keeping torques. The gravity gradient torque is usually negligible at GEO altitude, since it decreases with the inverse cubic power of the distance from the Earth [17]. The solar radiation pressure torque depends on the orientation of the solar panels. Since the solar panels rotate at a rate of one rotation per day to track the sun, the resulting disturbance is characterized by daily quasiperiodic oscillations with a torque amplitude that depends on the offset between the center of mass of the spacecraft and the center of solar pressure. Moreover, this disturbance vanishes during eclipses. The disturbance torque arising from station-keeping operations depends on both the offset of the center of mass with respect to the nominal position and the misalignment of the EP thrust vector from the nominal direction. By simulating a realistic weekly station-keeping cycle, with one day devoted to orbit determination followed by six consequent days of pre-planned maneuvers [18], it turns out that the maximum magnitude of the stationkeeping disturbance torque is much greater than that of the environmental torques. The geometry of a north/south maneuver is depicted in Figure 2, where the EP thrusters are fired in correspondence of circular arcs around the orbit nodes. During most of the orbital period, the spacecraft is allowed to drift with respect to the nominal orbit and experiences small environmental torques only, while a significant persistent torque is generated during orbit correction maneuvers. This is clearly visible in Figure 3 which shows the disturbance torques acting on the pitch axis, for a typical worst-case simulation with respect to the thruster alignment and center of mass offset (notice the different magnitudes of the torques).

IV. ATTITUDE CONTROL

The purpose of the ACS is to track the LVLH reference trajectory within the prescribed accuracy, while minimizing the fuel consumption and the overall number of thruster firings. The reference attitude consists of: (i) the quaternion $\bar{\mathbf{q}}_{IL}$, which is periodically uploaded from ground stations and defines the orientation of the LVLH frame with respect

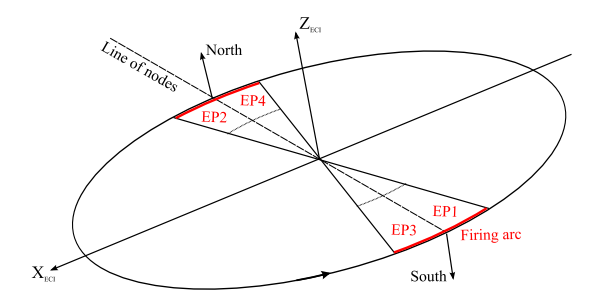


Fig. 2. North/south station-keeping maneuver

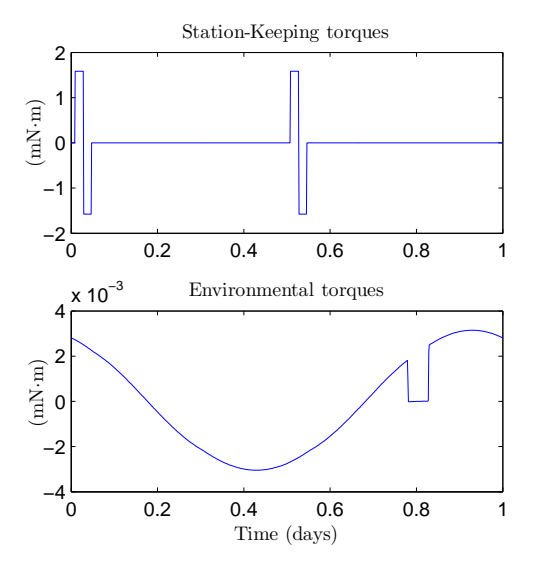


Fig. 3. Disturbance torques on the pitch axis

to the ECI frame; (ii) the LVLH frame rotation rate, given by

$$\bar{\boldsymbol{\omega}}_L = \begin{bmatrix} 0, -\omega_L, 0 \end{bmatrix}^T, \tag{6}$$

where ω_L is the constant orbit rate. An MPC-based approach is proposed, which explicitly incorporates the limitations on pointing and pointing rate accuracy. A suitable trade-off between fuel consumption and number of thruster firings is introduced in the cost function. Due to the presence of on/off actuators, the problem requires the solution of a mixed-integer linear program within a receding horizon control scheme.

A. Error dynamics

The plant model consists of a discrete-time linear approximation of the attitude error dynamics. If the attitude error with respect to the reference LVLH frame is small, it can be approximated by the three-dimensional rotation vector $\delta \theta$, which is obtained from the vector part of the attitude error quaternion as

$$\begin{bmatrix} 1 \\ \delta \boldsymbol{\theta} / 2 \end{bmatrix} = \delta \mathbf{q} (\delta \boldsymbol{\theta}) \approx \mathbf{q}_{IB} \circ \bar{\mathbf{q}}_{LI}, \tag{7}$$

where the right hand side represents the rotation from the LVLH frame to the body frame. The angular rate error is

given by the difference between the body frame and the LVLH frame rotation rates, expressed in the body frame

$$\delta \boldsymbol{\omega} = \boldsymbol{\omega} - \mathbf{R}(\mathbf{q}_{IB}) \mathbf{R}(\bar{\mathbf{q}}_{IL})^T \, \bar{\boldsymbol{\omega}}_L. \tag{8}$$

Assuming small angles and small angular rates, one has

$$\delta \dot{\boldsymbol{\theta}} = \delta \boldsymbol{\omega}. \tag{9}$$

Hence, the linearized model can be cast in the state space form as

$$\dot{\mathbf{x}} = \mathbf{A}\,\mathbf{x} + \mathbf{B}\,\mathbf{u} + \mathbf{B}_d\,\boldsymbol{\tau}_d,\tag{10}$$

where $\mathbf{x} = \begin{bmatrix} \delta \boldsymbol{\theta}^T \ \delta \boldsymbol{\omega}^T \end{bmatrix}^T$. The state matrix is given by

$$\mathbf{A} = \begin{bmatrix} \mathbf{0}_3 & \mathbf{I}_3 \\ \mathbf{0}_3 & \mathbf{A}_{\boldsymbol{\omega}} \end{bmatrix},\tag{11}$$

where \mathbf{A}_{ω} represents the cross-coupling contribution due to the rotation of the LVLH frame. By using a constant approximation of the inertia matrix $\overline{\mathbf{I}}_{\mathbf{M}} = \operatorname{diag}([I_x, I_y, I_z])$, through long but standard manipulations of (1)-(2) and (8) (see, e.g., [19]), one obtains

$$\mathbf{A}_{\omega} = \begin{bmatrix} 0 & 0 & \frac{I_x - I_y + I_z}{I_x} \, \omega_L \\ 0 & 0 & 0 \\ \frac{I_y - I_x - I_z}{I_z} \, \omega_L & 0 & 0 \end{bmatrix} . \tag{12}$$

The input matrices can be expressed as

$$\mathbf{B} = \begin{bmatrix} \mathbf{0}_{3 \times 6} \\ \overline{\mathbf{I}}_{\mathbf{M}}^{-1} \mathbf{T} \end{bmatrix}, \qquad \mathbf{B}_d = \begin{bmatrix} \mathbf{0}_3 \\ \overline{\mathbf{I}}_{\mathbf{M}}^{-1} \end{bmatrix}, \qquad (13)$$

where the matrix T is given by (4). The continuous time model is discretized with a sampling time Δt_s , thus obtaining

$$\mathbf{x}(t+1) = \mathbf{F}\,\mathbf{x}(t) + \mathbf{G}\,\mathbf{u}(t) + \mathbf{G}_d\,\boldsymbol{\tau}_d(t),\tag{14}$$

with

$$\mathbf{F} = e^{\mathbf{A}\Delta t_s},$$

$$\mathbf{G} = \left(\int_0^{\Delta t_s} e^{\mathbf{A}\rho} d\rho\right) \mathbf{B},$$

$$\mathbf{G}_d = \left(\int_0^{\Delta t_s} e^{\mathbf{A}\rho} d\rho\right) \mathbf{B}_d.$$

The simplest approach to account for the minimum duration of thruster firings is to set the sampling time Δt_s equal to or grater than the minimum firing time of the thrusters. Such a choice is a viable solution for the considered CGT/VHTR technology since the resulting sampling time is fully compatible with an accurate system discretization for control purposes. Should the minimum switching time imposed by the thruster technology be excessively large for discretization purposes, techniques like the one proposed in [15], allowing one to explicitly include switching-time constraints in the control design problem, can be adopted.

B. Control synthesis

The control accuracy requirements discussed in Section II can be formulated as:

$$\|\delta\boldsymbol{\theta}\|_{\infty} \leq \theta_{\max}, \\ \|\delta\boldsymbol{\omega}\|_{\infty} \leq \omega_{\max}.$$
 (15)

According to (5), a cost function proportional to the amount of expended fuel from time t to time t + N is given by:

$$J_1(\mathbf{U}_t, N) = \sum_{k=0}^{N} \| \mathbf{\Lambda} \mathbf{u}(t+k) \|_1$$
 (16)

where $\mathbf{U}_t = \{\mathbf{u}(t), \dots, \mathbf{u}(t+N)\}$ is the input sequence on the considered control horizon. Moreover, being $u_i \in \{0, 1\}$, the number of thruster switchings, which accounts for thruster valve wear, can be expressed as:

$$J_2(\mathbf{U}_t, N) = \sum_{k=0}^{N} \| \mathbf{\Lambda} [\mathbf{u}(t+k) - \mathbf{u}(t+k-1)] \|_1.$$
 (17)

Given a state vector $\mathbf{x}(t)$, the computation of the control input sequence \mathbf{U}_t at time t can be formulated as an optimization problem of the form:

$$\min_{\mathbf{U}_{t}} \quad (1-\alpha) J_{1}(\mathbf{U}_{t}, N) + \alpha J_{2}(\mathbf{U}_{t}, N)$$
s.t.
$$\mathbf{x}(t+k+1) = \mathbf{F} \mathbf{x}(t+k) + \mathbf{G} \mathbf{u}(t+k) + \mathbf{G} \mathbf{u}(t+k)$$

$$+ \mathbf{G}_{d} \boldsymbol{\tau}_{d}(t+k)$$

$$\parallel \mathbf{D} \mathbf{x}(t+k) \parallel_{\infty} \leq 1$$

$$\mathbf{M} \mathbf{u}(t+k) \leq \mathbf{1}$$

$$u_{i}(t+k) \in \{0, 1\} \ \forall i \quad k = 0, \dots, N$$
(18)

where $\alpha \in [0, 1]$ is a relative weight of the terms J_1 and J_2 ,

$$\mathbf{D} = \begin{bmatrix} \mathbf{I}_3 / \theta_{\text{max}} & \mathbf{0}_3 \\ \mathbf{0}_3 & \mathbf{I}_3 / \omega_{\text{max}} \end{bmatrix}$$
 (19)

accounts for control accuracy requirements, and the constraint matrix

$$\mathbf{M} = \begin{bmatrix} 1 & 0 & 0 & 1 & 0 & 0 \\ 0 & 1 & 1 & 0 & 0 & 0 \\ 0 & 0 & 0 & 0 & 1 & 1 \end{bmatrix}$$
 (20)

is introduced to prevent control inputs resulting in torques summing up to zero.

In a receding horizon control strategy, one has to solve problem (18) at each time t and then apply the first element $\mathbf{u}(t)$ of the computed input sequence \mathbf{U}_t . In order to solve problem (18), an estimate of the initial state $\mathbf{x}(t)$ and of the disturbance torque $\boldsymbol{\tau}_d(t+k)$, $k=0,\ldots,N-1$, must be available. Since the disturbance torque depends on thruster misalignment and center of mass position, one can assume that it is constant over the considered control horizon and treat it as an uncertain parameter to be estimated. Then, an extended Kalman filter (EKF) is used to estimate both the state $\mathbf{x}(t)$ and the disturbance torque $\boldsymbol{\tau}_d$, by using combined gyro and star-tracker measurements [20]. The resulting closed-loop system is depicted in Figure 4, where $\hat{\mathbf{q}}_{IB}$, $\hat{\boldsymbol{\omega}}$ and $\hat{\boldsymbol{\tau}}_d$ denote the estimates of the spacecraft attitude, rotation rate and disturbance torque, respectively.

In order to ensure feasibility in the presence of estimation errors and model uncertainties, the state constraints in problem (18) are relaxed by introducing slack variables and penalizing them in the cost function [21], [22]. Such relaxation is motivated by the fact that small violations of the error constraints can be tolerated for short time periods,

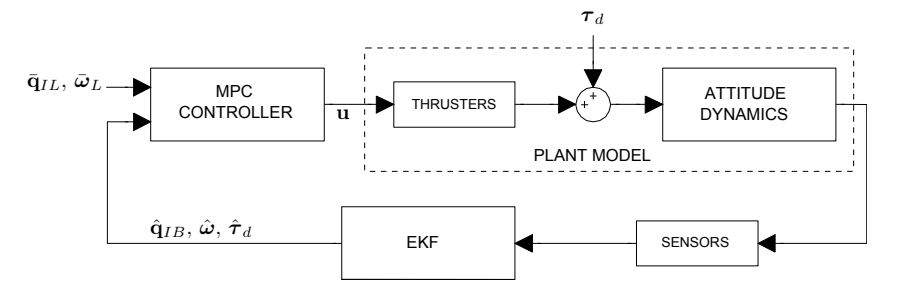


Fig. 4. Closed-loop system

given rather conservative bounds on the pointing and pointing rate accuracy. Hence, problem (18) can be reformulated as

$$\min_{\mathbf{U}_{t}, \mathbf{S}} \quad (1 - \alpha) J_{1}(\mathbf{U}_{t}, N_{u} - 1) + \alpha J_{2}(\mathbf{U}_{t}, N_{u} - 1) \\
+ \sum_{k=1}^{N_{x} - 1} \| \mathbf{K}_{s} \mathbf{s}_{t+k} \|_{1} + \| \mathbf{K}_{x} \mathbf{x}_{t+N_{x}} \|_{1} \\
\text{s.t.} \quad \mathbf{x}_{t} = \hat{\mathbf{x}}(t) \\
\mathbf{x}_{t+k+1} = \mathbf{F} \mathbf{x}_{t+k} + \mathbf{G} \mathbf{u}_{t+k} + \mathbf{G}_{d} \hat{\tau}_{d} \\
- 1 - \mathbf{D} \mathbf{s}_{t+k} \leq \mathbf{D} \mathbf{x}_{t+k} \leq 1 + \mathbf{D} \mathbf{s}_{t+k} \\
\mathbf{s}_{t+k} \geq \mathbf{0} \\
\mathbf{M} \mathbf{u}_{t+k} \leq \mathbf{1} \\
u_{t+k,i} \in \{0, 1\} \quad \forall i, \forall k = 0, \dots, N_{x} - 1 \\
\mathbf{u}_{t+N_{y}} = \dots = \mathbf{u}_{t+N_{x} - 1} = \mathbf{0}$$

where $\hat{\mathbf{x}}(t)$ is the estimate of the error state vector $\mathbf{x}(t)$ returned by the EKF. The weight on the terminal state \mathbf{K}_x is a standard tool in MPC, which favours stability of the receding horizon control strategy [23], while matrix K_s is introduced to penalize the weighted ℓ_1 -norm of the slack variables $\mathbf{S} = \{\mathbf{s}_{t+1}, \dots, \mathbf{s}_{t+N_x-1}\}$. It is worth noticing that in problem (21), the control horizon N_u is different from the prediction horizon N_x , with $N_u \leq N_x$. After the first N_u samples, the control variables are set to zero while the state constraints are enforced also in the subsequent $N_x - N_u$ samples. This allows one to suitably trade-off the number of optimization variables and the performance of the ACS. In fact, problem (21) is a MILP problem which is known to be computationally intractable in the general case [24]. Nevertheless, if the control horizon is kept short enough, state-of-the-art MILP algorithms can provide an approximate solution in a reasonable amount of time. In this work, the IBM ILOG CPLEX mixed-integer programming solver [25], based on a branch and bound algorithm, has been employed to solve problem (21).

V. SIMULATION RESULTS

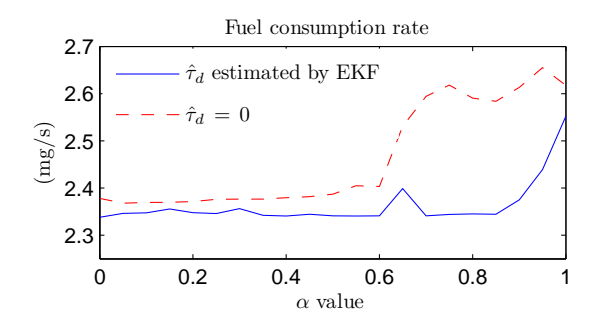
In order to evaluate the performance of the MPC-based control law proposed in Section IV, a sample GEO mission is numerically simulated (see Table II). To this purpose, a high-fidelity simulator has been developed, combining a realistic model of the spacecraft dynamics with a navigation system relying upon an EKF for state estimation. A number

TABLE II GEO reference orbit

Semi-major axis	a	=42165 (km)
Inclination	i	$\in [0, 0.05] \text{ (deg)}$
Longitude	λ	$\in [75.05, 75.15]$ (deg)
Eccentricity	e	$\simeq 0$

of uncertainty sources and disturbance effects, affecting the real spacecraft dynamics, are included in the simulation model. Both the spacecraft mass and inertia matrix are timevarying due to propellant expulsion and moving parts. The actual center of mass and the thruster alignment are allowed to differ from the nominal values up to 2 cm and 0.6°, respectively. Disturbance accelerations due to solar radiation pressure, aspherical and third body gravity are taken into account. Disturbance torques resulting from gravity gradient, solar radiation pressure (taking into account the rotation of the solar panels) and EP thrusters misalignment are also considered. A multiplicative extended Kalman filter takes care of estimating the spacecraft attitude and angular velocity from star-tracker and gyro measurements. As an additional output, the EKF yields an estimate of the disturbance torque resulting from the station-keeping maneuvers, which is used by the MPC controller.

The error bounds in (15) are set to $\theta_{\text{max}} = 0.9$ mrad and $\omega_{\rm max} = 9 \, \mu {\rm rad/s}$, with a 10% safety margin with respect to the mission requirements in order to account for constraint relaxation in the MPC formulation. The tuning parameters of the controller are N_u , N_x , \mathbf{K}_s , \mathbf{K}_x and α in (21). The control horizon N_u , which is proportional to the number of binary variables in the optimization problem, has the major impact on the computational burden of the control system. Since the amount of computational resources available onboard a spacecraft is typically limited, $N_u = 3$ has been chosen. A prediction horizon three times longer than the control horizon has been selected, by setting $N_x = 9$. The penalty term K_s , which affects the constraint violations, has been chosen as a block diagonal matrix $\mathbf{K}_s = \text{blockdiag}(3 \cdot$ $10^5\,\mathbf{I}_2,~2\cdot 10^5,~3\cdot 10^5\,\mathbf{I}_2,~2\cdot 10^5),$ while the terminal weight has been set to $\mathbf{K}_x = \mathbf{K}_s/10$. Finally, the parameter α determines the relative weight of the fuel consumption and the number of thruster firings in the cost function of the



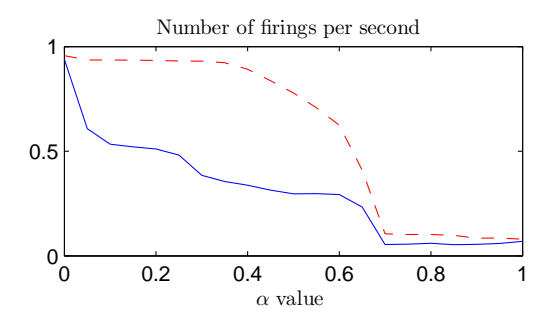


Fig. 5. Tuning of parameter α

optimization problem. In order to find a suitable value of α , several station-keeping maneuvers on a GEO orbit have been simulated, with α ranging from zero to one. A worst-case scenario has been considered, by assuming the maximum disturbance torque τ_d compatible with the uncertainty on the center of mass and thruster misalignment. The results are depicted in Figure 5, where the fuel consumption rate and the number of thruster firings per second are reported. As expected, the parameter α serves to trade-off between the two conflicting objectives. It can be noticed that the fuel consumption is approximately constant as long as α is smaller than 0.85, while it rapidly grows as α approaches 1. Conversely, an acceptable number of firings is achieved only if α is larger than 0.7. From these observations, $\alpha = 0.8$ has been selected. Figure 5 also reports the same quantities in case the disturbance torque τ_d is not estimated and $\hat{\tau}_d = 0$ is used in the control problem (21). It can be seen that estimating τ_d provides a significantly improvement in the performance, both in terms of fuel consumption and number of firings, as expected.

A sampling time $\Delta t_s=0.5~s$ has been chosen. Such a value is adequate for discretizing the spacecraft dynamic model and is well within the constraints on the minimum firing time imposed by the thruster technology. This combination of parameters provides an average computational time of the control law in the millisecond range, using the CPLEX solver on a 2 GHz single-core CPU.

The proposed ACS is compared to a different control scheme, consisting of the cascade of a LQR controller and a quantizer. Both a static binary quantizer (BQ) and a PWPF modulator have been considered. A preliminary study is reported in Figure 6, where the performance of the two LQR-based controllers on the yaw axis is compared. Both the scheme with the static quantizer (LQR+BQ) and the one with the PWPF modulator (LQR+PWPF) are able to keep the attitude and angular rate errors within the prescribed bounds, and show a similar behavior in terms of fuel consumption. However, the LQR+BQ scheme requires a much higher number of thruster firings, due to the lack of hysteresis in the quantization mechanism. Hence, only the LQR+PWPF is considered in the subsequent comparisons. This preliminary analysis clearly shows that in the considered scenario the number of thruster firings is a key issue to be taken into account in the design of the control law.

A typical transient response of the MPC-based control scheme with respect to large initial attitude and angular rate errors is reported in Figure 7 for the yaw axis (similar behaviors are observed for the other axes). In this simulation the main disturbance torque acts along the negative yaw direction. The controller is able to drive the tracking errors within the bounds (dash-dotted lines). The steady state behavior of the MPC-based ACS is compared to that of the LQR+PWPF scheme in Figure 8. It can be observed that both controllers succeed in keeping the errors within the bounds, for all axes. Clearly, an advantage of the MPC approach is that such bounds are enforced directly as constraints in the optimization problem (21), while a trial-and-error procedure has been necessary to suitably tune the parameters of the LQR+PWPF controller to this purpose.

The performance of the two ACSs in terms of fuel consumption and number of thruster firings is reported in Figure 9. The fuel consumption does not show an appreciable difference between the two approaches, but the MPC scheme requires about 25% less thruster firings with respect to the LQR+PWPF one, mainly due to a more efficient management of the firing cycles for the cross-coupled axes (roll and pitch). A longer simulation, lasting one week, has also been performed for the MPC control law, in order to estimate the fuel consumption and the number of thruster firings that would be required for precise attitude control of an allelectric spacecraft over the entire mission lifetime. Results indicate that about 95 Kg of additional Xenon propellant onboard the spacecraft would guarantee a mission duration of about 15 years, with a number of firing cycles in the range of one million per thruster, which is compatible with the considered CGT/VHTR technology.

VI. CONCLUSIONS

Simulation results demonstrate that cold gas and resistojet technologies, in combination with the proposed attitude control scheme, can be effective for three-axis precision pointing of an all-electric GEO spacecraft. The control system is able to counteract disturbance torques of persisting nature, while keeping the attitude and angular rate within prescribed bounds. Thrusters limitations are explicitly accounted for in the control system design phase, to provide efficient management of the thruster firings without significant impact on the fuel consumption. The proposed approach allows

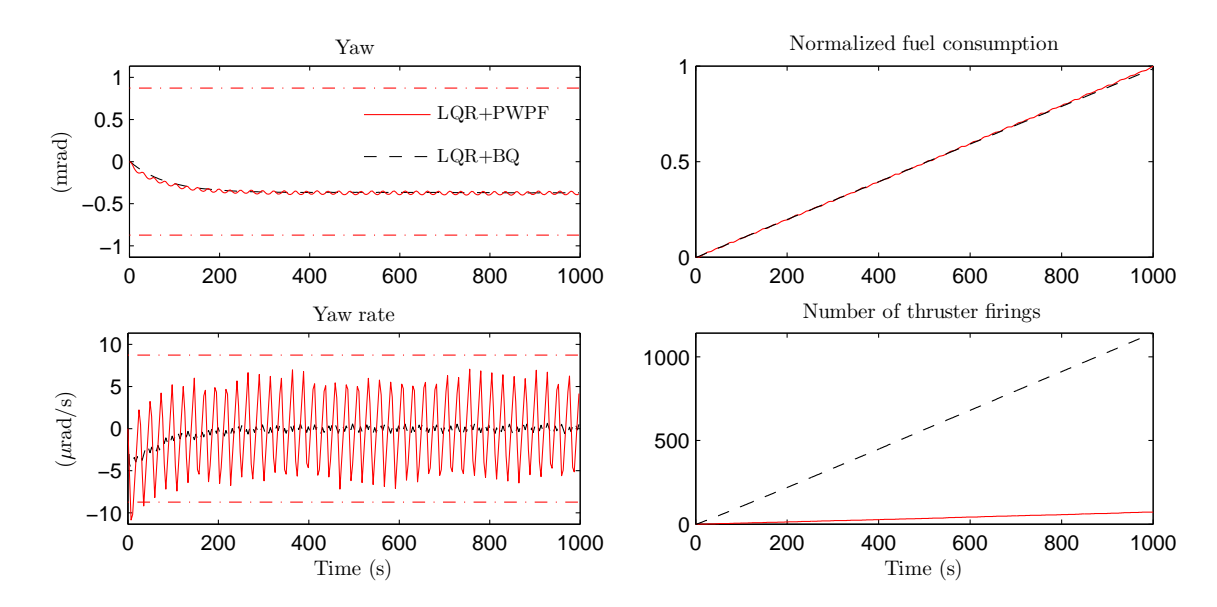


Fig. 6. Comparison of LQR+BQ and LQR+PWPF control schemes

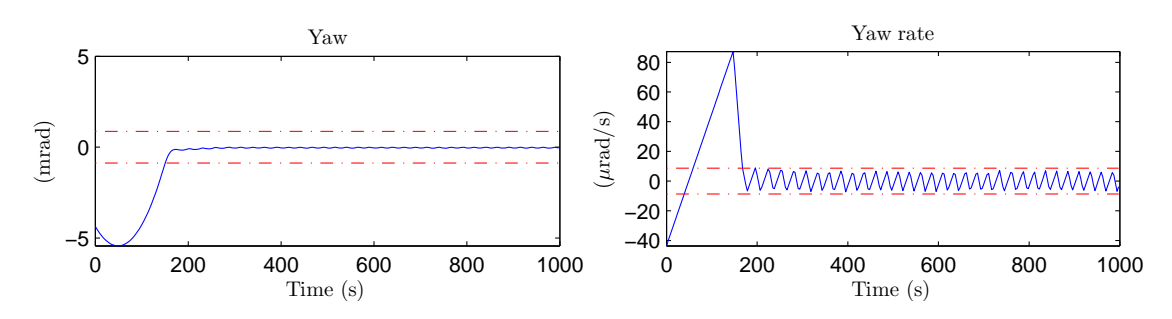


Fig. 7. Transient behavior of the MPC tracking error: Yaw axis

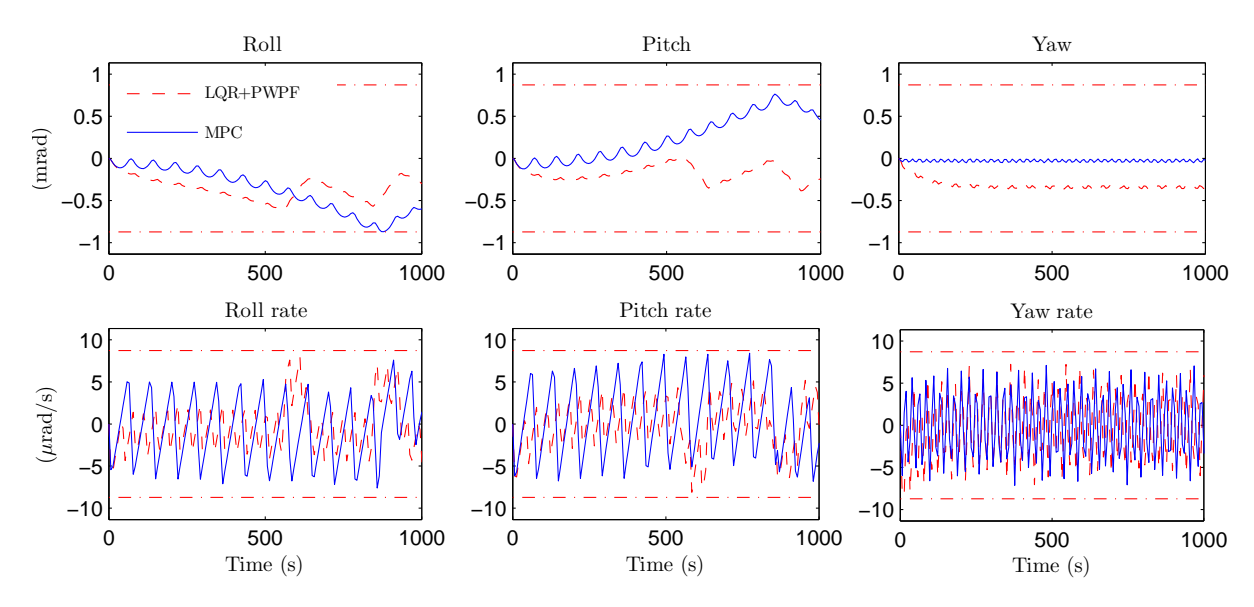
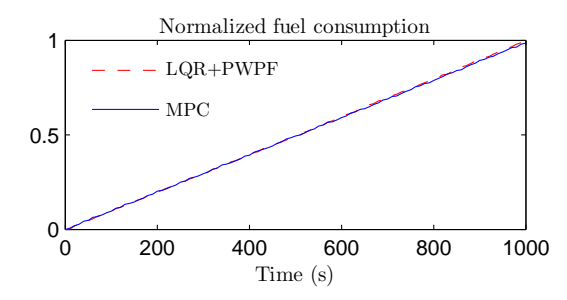


Fig. 8. MPC and LQR+PWPF tracking errors in steady-state



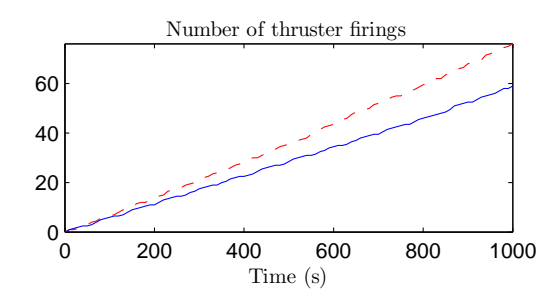


Fig. 9. MPC and LQR+PWPF performance: Fuel consumption and number of firings

one to trade-off these conflicting objectives, by suitably triggering the cost function parameter α . The use of a time-varying α along the orbit is the subject of ongoing studies. It is believed that it may provide further performance improvements, being quite different the nature and size of the disturbance torques caused by station-keeping maneuvers and environmental disturbances. Robustness analysis with respect to parametric uncertainty is a subject of current research. Alternative control techniques, such as explicit MPC possibly combined with a PWPF modulator, are also under investigation.

REFERENCES

- [1] J. Gonzalez and G. Saccoccia. ESA Electric Propulsion activities. In 32nd International Electric Propulsion Conference, 2011.
- [2] Boeing 702SP satellite. http://www.boeing.com/defense-space/space/bss/factsheets/702/702SP.html.
- [3] P. Patel, D Scheeres, and A. Gallimore. Maximizing payload mass fractions of spacecraft for interplanetary electric propulsion missions. *Journal of Spacecraft and Rockets*, 43(4):822–827, 2006.
- [4] D. Manzella. Low Cost Electric Propulsion Thruster for Deep Space Robotic Missions. In 2007 NASA Science Technology Conference, Hyattsville, Maryland, June 2007. Paper No. 07-0116.
- [5] A. Garulli, A. Giannitrapani, M. Leomanni, and F. Scortecci. Autonomous low-Earth-orbit station-keeping with electric propulsion. *Journal of Guidance Control and Dynamics*, 34(6):1683–1693, 2011.
- [6] D. Nicolini, D. Robertson, E. Chesta, G. Saccoccia, D. Gibbon, and A. M. Baker. Xenon resistojets as a secondary propulsion on EP spacecrafts and performance results of resistojets using Xenon. In 28th International Electric Propulsion Conference, 2003.
- [7] M. Coletti, A. Grubisic, C. Collingwood, and S. Gabriel. Electric propulsion subsystem architecture for an all-electric spacecraft. In J. Hall, editor, *Advances in Spacecraft Technologies*, pages 123–138. InTech, 2011.
- [8] N.M.F. Oliveira and K.H. Kienitz. Attitude controller design for a system using actuators with switching-time restrictions and delays. In AIAA Guidance, Navigation, and Control Conference, 2000.
- [9] S.J. Dodds and S.E. Williamson. A signed switching time bangbang attitude control law for fine pointing of flexible spacecraft. *International Journal of Control*, 40(4):795–811, 1984.

- [10] B.N. Agrawal, R.S. Mcclelland, and G. Song. Attitude control of flexible spacecraft using pulse-width pulse-frequency modulated thrusters. *Space Technology*, 17(1):15–34, 1997.
- [11] G. Arantes, L.S. Martins-Filho, and A.C. Santana. Optimal onoff attitude control for the Brazilian multimission platform satellite. *Mathematical Problems in Engineering*, vol. 2009, 2009.
- [12] T.D. Krovel. Optimal tuning of PWPF modulator for attitude control. PhD thesis, Norwegian University of Science and Technology, 2009.
- [13] D.B. Doman, B.J. Gamble, and A.D. Ngo. Control allocation of reaction control jets and aerodynamic surfaces for entry vehicles. In AIAA Guidance, Navigation and Control Conference and Exhibit, 2007
- [14] Ø. Hegrenæs, J.T. Gravdahl, and P. Tøndel. Spacecraft attitude control using explicit model predictive control. *Automatica*, 41(12):2107– 2114, 2005.
- [15] M.S. Vieira, R.K.H. Galvao, and K.H. Kienitz. Attitude stabilization with actuators subject to switching-time constraints using explicit MPC. In *IEEE Aerospace Conference*, 2011.
- [16] J.M. Shim. Korea geostationary satellite program: Communication, ocean, and meteorological satellite (COMS). In The 2006 EUMETSAT Meteorological Satellite Conference, 2006.
- [17] J.R. Wertz. Spacecraft attitude determination and control, pages 566–576. Reidel Publishing Company, 1978.
- [18] S. Berge, A. Edfors, T. Olsson, G. Pionnier, M. Björk, C. Chasset, T. Nordebäck, M. Rieschel, B. Lübke-Ossenbeck, and P. Zentgraf. Advanced AOCS design on the first Small GEO telecom satellite. In 60th International Astronautical Congress, 2009.
- [19] M.J. Sidi. Spacecraft dynamics and control: a practical engineering approach, volume 7, pages 107–111. 2000.
- [20] J.L. Crassidis, F.L. Markley, and Y. Cheng. Survey of nonlinear attitude estimation methods. *Journal of Guidance Gontrol and Dynamics*, 30(1):12–28, 2007.
- [21] J.M. Maciejowski. Predictive control with constraints. Pearson education, 2002.
- [22] M.N. Zeilinger, C.N. Jones, and M. Morari. Robust stability properties of soft constrained MPC. In 49th IEEE Conference on Decision and Control, pages 5276–5282, 2010.
- [23] D.Q. Mayne, J.B. Rawlings, C.V. Rao, and P.O.M. Scokaert. Constrained model predictive control: Stability and optimality. *Automatica*, 36(6):789–814, 2000.
- [24] F. Borrelli, M. Baotić, A. Bemporad, and M. Morari. Dynamic programming for constrained optimal control of discrete-time linear hybrid systems. *Automatica*, 41(10):1709–1721, 2005.
- [25] IBM. CPLEX, ILOG 11.0 User's Manual. ILOG CPLEX Division. Incline Village, NV, 2007.